Development of an Ultra-Cold Atom Atomic Clock

A thesis submitted in partial fulfillment of the requirement
for the degree of Bachelor of Science in Physics from
The College of William and Mary

by

Alexander Gvakharia

Accepted for __Honors__
(Honors, No Honors)

Seth Aubin, Advisor

Henry Krakauer, Director

Peter Kemper

Williamsburg, VA
April 25, 2012

Development of an Ultra-Cold Atom Atomic Clock: A Progress Report

Alexander Gvakharia

April 13th, 2012

Abstract

This thesis presents work on the development of an atomic clock using bosonic potassium (^{39}K and ^{87}Rb) in order to study the role of inter-atom interactions on an atomic time standard. The project designed and constructed an RF circuit and RF antenna to manipulate the internal hyperfine states of the ultra-cold atoms. We developed an optical trap to trap these atoms in a vacuum cell, and performed several tests to check their behavior and measure their temperature. We performed experiments to observe Rabi flopping between the hyperfine states of the atoms. The eventual goal of this project is to create an operational atomic clock and observe the effects of inter-atom interactions.

Contents

1 Introduction

Atomic clocks are the most accurate time-keeping devices available, capable of keeping time at the level of 1 part in 10^{11} to 1 part in 10^{17} [1]. Furthermore, they play a key role in the global positioning system and space navigation, applications that require extremely high accuracy. The current official worldwide time standard uses an atom fountain atomic clock. For a fountain, multiple lasers are used to trap atoms in optical molasses. The atoms are then accelerated vertically by more lasers through a microwave-filled cavity and allowed to fall down. During this "fountain" motion, if any of the atoms change states due to the microwaves, they will emit photons which are detected. At the right resonant frequency of the microwaves, the fluorescence is maximized and this sets the time [2]. In a generic atomic clock, a radio frequency pulse is applied to optically trapped atoms, altering their states. After waiting a time corresponding to the transition period of the atom, a second pulse is used to probe the system. With perfect timing, the atoms should be equally split between ground and excited states, and so the frequency of the pulse can be adjusted to achieve resonance.

Current atomic clocks are limited by inter-atom interactions. For ultra-cold bosonic (integer spin) atoms, collisions between the atoms affect the frequency of the hyperfine splitting, the reference frequency for the clock, and thus become more important at high precision. It is difficult to control the density of the trapped atoms, which leads to an inconsistent offset in the transition frequency. Ultra-cold fermionic (half-integer spin) atoms do not experience inter-atom interactions. As the temperature decreases, the fermions approach degeneracy by occupying all possible energy levels. The Paul Exclusion principle prevents two fermions from occupying the same energy level and prohibits indistinguishable fermions from colliding [3]. Building an atomic clock will allow measurement and observation of inter-atom interactions, providing an additional experimental means of probing them. An external magnetic field can be tuned to a Feshbach resonance which alters the scattering length of a collision,

allowing tuning of inter-atom interactions [4]. The development of a bosonic atom clock will lead to an eventual fermionic atom clock, in which inter-atom interactions are strongly suppressed.

2 Theory

2.1 Atomic Clock Operation

The clock will use ultra-cold atoms that are laser-cooled to below 100 μK in an optical dipole trap. A diagram of the experimental set-up is given by Figure 2.1.
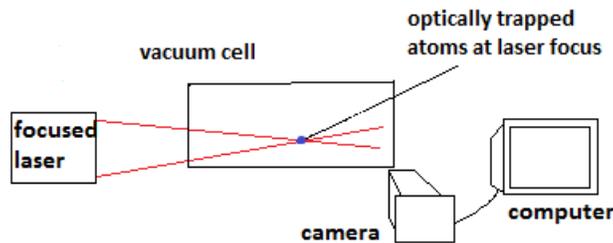

Figure 2.1: Sketch of the clock setup. The focused laser traps the atoms in the vacuum cell. The atoms are then probed and imaged with the camera

The atoms are all prepared in the same internal quantum state, after which a radio-frequency $\pi/2$ pulse is applied which places the atoms in a superposition of two quantum states. The atomic spins are allowed to precess at the hyperfine splitting frequency for a fixed time, after which a second $\pi/2$ pulse stops the clock. The frequency for ^{39}K is 461.7 MHz, and for ^{41}K, it is 254.0 MHz. The $\pi/2$ pulse timing and frequency are set by a voltage-controlled 10 MHz clock. When the system is interrogated with the second pulse, the atoms are observed to be in one of the two hyperfine states. The atom populations are measured by first spatially separating them with a magnetic or RF field and then imaging them. An outline of the steps is presented in Figure 2.2.
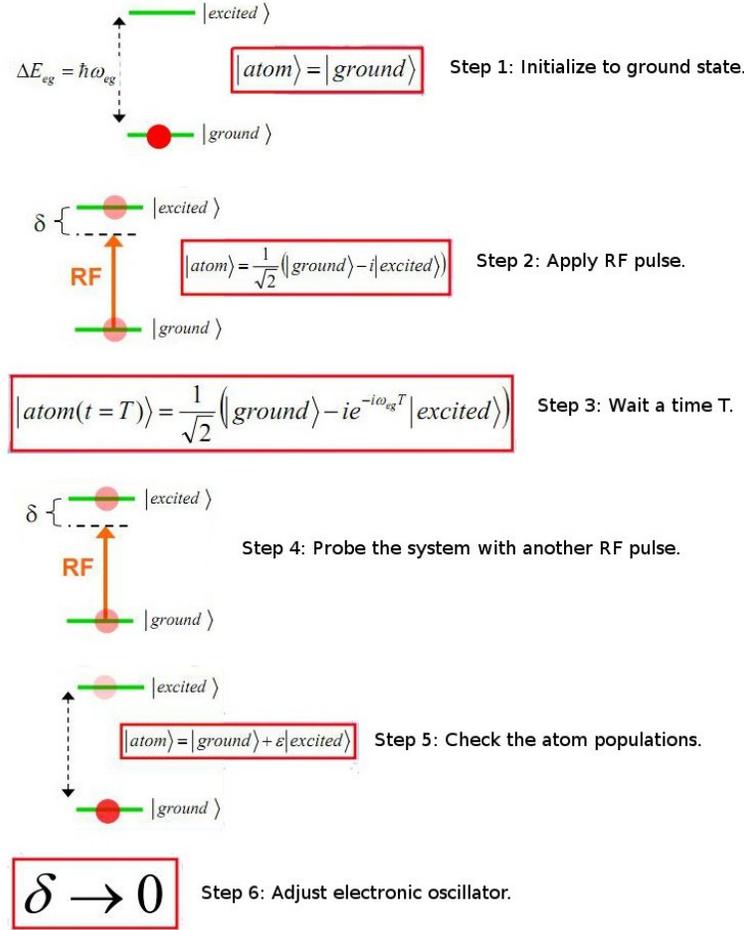
Figure 2.2: The steps to the atomic clock operation. First, the atoms are initialized in the ground state (1). Then, a $\pi/2$ RF pulse is applied which places the atoms in a superposition of states (2). After waiting a time T (3), the system is probed with another $\pi/2$ RF pulse (4). The atoms are imaged and their population densities are compared (5). If the detuning is off-resonance, the atom populations will be unequal. The detuning is adjusted accordingly (6). [Figures adapted from Seth Aubin.]

The relative populations of the two hyperfine states determine the offset of the electronic oscillator from the hyperfine transition frequency, so that a negative feedback loop can be used to periodically correct the frequency of the electronic oscillator to match the hyperfine splitting frequency. In this manner, the electronic oscillator frequency is locked to the hyperfine splitting, and so ensures that the atoms are equally split between the two states. Figure 2.3 shows the layout of the clocking process.

The necessary technical steps for creating the atomic clock are optically trapping the

atoms, optically pumping them into an initial state, and manipulating them with $\pi/2$ pulses to observe Rabi flopping. These steps are explained in the subsequent sections.
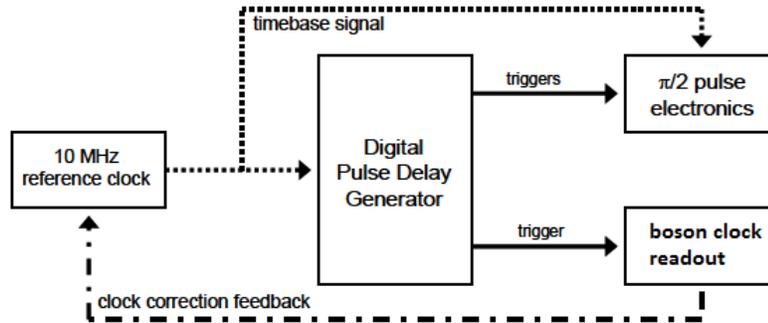

Figure 2.3: Diagram of the clocking algorithm [Figure adapted from Prof. Seth Aubin.]

2.2 Inter-atom Interactions

The atomic clock will be used to investigate the effect of inter-atom interactions on the hyperfine splitting and clock frequency of a ^{39}K (and time permitting, ^{41}K) atomic clock. A magnetic Feshbach resonance can be used to tune the atom-atom interaction strength. For initial clocking, the atoms are in the $|F = 2, m_F = 0>$ and $|F = 1, m_F = 0>$ states, where F is the total angular momentum of the nucleus and m_F is the projection of the spin on the quantization axis. These states are the least susceptible to influence from a magnetic field. To employ a Feshbach resonance, we use the $|F = 2, m_F = +1>$ and $|F = 1, m_F = -1>$ states of ^{41}K. When an external magnetic field is applied near a Feshbach resonance, atom-atom interaction becomes noticeably large. A sketch of the energy shifts is shown in Figure 2.4. The energy shift affects the hyperfine splitting frequency, which disrupts the timing of the atomic clock.
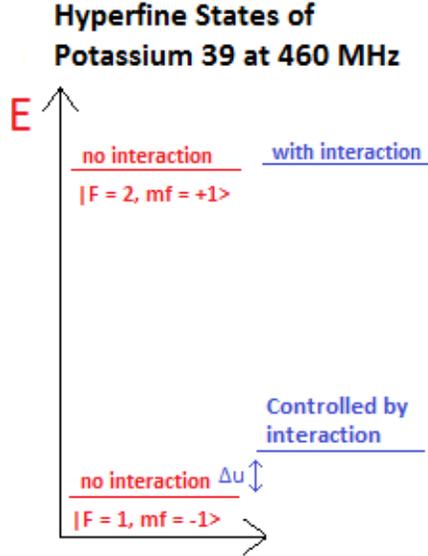
Figure 2.4: Energy splitting as a result of magnetic Feshbach resonance. A magnetic field tuned to the resonance strength will cause a noticeable shift in the ground state energy level, which can be adjusted.

2.3 Optical Trap Theory

The atoms will be held in a dipole trap. The dipole trap operates by using a focused laser beam at an optical frequency that is off from the frequency of one of the atom states, either the ground or the excited. Blue-detuned traps use a frequency that is slightly higher than the resonant frequency, while red-detuned uses a frequency that is lower. We will use red-detuning. This creates an area of low potential, which attracts the atoms. The focal area also has a certain width, or waist, illustrated in Figure 2.5. The formula for the trap potential, or depth, is given by

$$U_{dipole} = \frac{\hbar\Gamma}{8} \frac{\Gamma}{\delta} \frac{I}{I_{sat}} \tag{2.1}$$

where Γ is full-width at half-maximum of the atomic transition linewidth, δ is the difference between the frequency of the laser and the frequency of the atomic transition, I is the intensity of the laser, and I_{sat} is the saturation intensity [5]. For Rubidium, $I_{sat} = 1.6$ mW/cm^2, and $\Gamma = 2\pi \times 6$ MHz. Rubidium will be used for initial testing. For Potassium, I_{sat}

$= 1.8$ mW/cm^2, and $\Gamma = 2\pi \times 6.1$ MHz. The intensity profile of the laser is approximately a Gaussian, given by [6]

$$I(r) = I_0 e^{-2\frac{r^2}{w_0^2}} \tag{2.2}$$

where w_0 is the full-width at half-maximum, around 50μm. We can integrate the intensity equation Equation 2.2 over an area to get the power, which for our laser is about 1W. So,

$$\int_0^{2\pi} \int_0^\infty I_0 e^{-2\frac{r^2}{w_0^2}} r \, dr \, d\theta = 1W \tag{2.3}$$

$$\Rightarrow \frac{\pi w_0^2 I_0}{2} = 1W \tag{2.4}$$

Thus, with $w_0 = 50\mu$m, $I_0 = 2.55 \times 10^8 \frac{W}{m^2}$. We can now use this value of I_0 in Equation 2.1 to find the trap depth. We also need to know the detuning δ. We operate at $\lambda = 800$ nm, and the transition wavelength $\lambda_{D1} = 795$ nm, so $\delta = 2\pi \times 1.48 \times 10^{13}$. We find $U_{dipole} = 2.0 \times 10^{-26}$J $=$ kT, where k is the Boltzmann constant, $1.38 \times 10^{-23} \frac{J}{K}$. So, $U_{dipole} = 1.45$ mK.
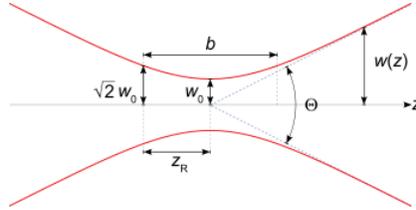

Figure 2.5: Illustration of a dipole trap beam, w_0 indicating the beam waist.

2.4 Rabi Flopping

Rabi flopping is a process by which an atom oscillates or "flops" through its energy levels in the presence of an external field, like a magnetic field or a laser. The atom undergoes stimulated emission and absorption to cyclically emit and absorb photons, and the length of the cycle is determined by the Rabi frequency. This Rabi frequency, Ω, depends on the

interaction Hamiltonian, and is defined as

$$\Omega = \frac{< g|H_{int}|e >}{\hbar} \tag{2.5}$$

The process also depends on the detuning, $\delta = \omega_{laser}$ - ω_{eg}, or the difference in frequency between the driving field and the transition. If the detuning is equal to 0 then the energy levels will oscillate at the specified Rabi frequency. If the detuning is off resonance, the Rabi flopping will be at a higher frequency, but weaker amplitude, and will oscillate at the generalized Rabi frequency,

$$\Omega' = \sqrt{\Omega^2 + \delta^2} \tag{2.6}$$

In order to observe flopping, we need to know the Rabi frequency. For an atom in a magnetic field, with $\Delta F = 0$, we can apply the appropriate Hamiltonian and then the Rabi frequency is given by

$$\Omega = \frac{\mu_B}{\hbar^2} g_F < F, m'_F|F_+\frac{B}{2} + F_-\frac{B}{2}|F, m_F > \tag{2.7}$$

Where B is our magnetic field, F_+ and F_- are the raising and lowering operators, μ_B is the magnetic moment, equal to $\hbar \times 1.4$ MHz/G, and g_F, the hyperfine Landé g-factor, is

$$g_F = g_J \frac{F(F+1) - I(I+1) + J(J+1)}{2F(F+1)} \tag{2.8}$$

and g_J, the Landé factor, is (after neglecting small terms)

$$g_J \simeq 1 + \frac{J(J+1) + S(S+1) - L(L+1)}{2J(J+1)} \tag{2.9}$$

For our system, F = 2, I = $\frac{3}{2}$, J = $\frac{1}{2}$, S = $\frac{1}{2}$, and L = 0. Then, $g_J = 2$, and $g_F = \frac{1}{2}$. For our transition, $m'_F = 2$, $m_F = 1$, and after applying the raising and lowering operators, we

obtain that

$$\Omega_{2\to1} = \frac{\mu_B g_F B}{\hbar} \tag{2.10}$$

The magnetic field B can be calculated by approximating the antenna to a current loop,

$$B_{loop} = \frac{\mu_0 I}{2R} \tag{2.11}$$

With our values of g_F and B, $\Omega \simeq 5.9$ kHz.

For $\Delta F = \pm 1$, we have to use Clebsch-Gordan coefficients in the calculation. The F states can be represented by F_+ and F_-, given by

$$|F_+ = I + S, m_F> = \frac{\sqrt{F_+ + m_F}}{\sqrt{2I + 1}}|m_I = m_F - \frac{1}{2}>|\uparrow> + \frac{\sqrt{F_+ - m_F}}{\sqrt{2I + 1}}|m_I = m_F + \frac{1}{2}>|\downarrow> \tag{2.12}$$

$$|F_- = I - S, m_F> = -\frac{\sqrt{F_+ - m_F}}{\sqrt{2I + 1}}|m_I = m_F - \frac{1}{2}>|\uparrow> + \frac{\sqrt{F_+ + m_F}}{\sqrt{2I + 1}}|m_I = m_F + \frac{1}{2}>|\downarrow> \tag{2.13}$$

For π-polarized light, with $\Delta m_F = 0$, the Rabi frequency is given by

$$\Omega = \frac{\mu_B}{\hbar^2} g_S |B_{AC}| <F', m'_F|S_z|F, m_F> \tag{2.14}$$

The S_z operator gives an eigenvalue of $\hbar m_s$, in this case $m_s = \frac{1}{2}$. The equation solves to give

$$\Omega = \frac{\mu_B}{\hbar^2} g_s |B_{AC}|(\frac{\sqrt{2 - m_F}\sqrt{2 + m_F}}{4}) \tag{2.15}$$

For σ-polarized light, $\Delta m_F = \pm 1$, the Rabi frequency is given by

$$\Omega = \frac{\mu_B}{\hbar^2} g_s <F', m'_F|S_+ B_{-AC} + S_- B_{+AC}|F, m_F> \tag{2.16}$$

The raising/lowering operators S_+ and S_- return $\hbar\sqrt{S(S + 1) - m(m \pm 1)}|S, m \pm 1>$

For F' = F$_-$, F = F$_+$, the S_+B_{-AC} matrix element is

$$\Omega = -\frac{\mu_B}{\hbar}g_s|\frac{B_{DC}}{2}|\frac{1}{2}\sqrt{2-m'_F}\sqrt{2-m_F} < m'_F - \frac{1}{2}|m_F + \frac{1}{2} > \qquad (2.17)$$

The S_-B_{+DC} matrix element is

$$\Omega = \frac{\mu_B}{\hbar}g_s|\frac{B_{DC}}{2}|\frac{1}{2}\sqrt{2+m'_F}\sqrt{2+m_F} < m'_F + \frac{1}{2}|m_F - \frac{1}{2} > \qquad (2.18)$$

With F' = F$_+$, F = F$_-$, the S_+B_{-AC} matrix element is

$$\Omega = -\frac{\mu_B}{\hbar}g_s|\frac{B_{DC}}{2}|\frac{1}{2}\sqrt{2-m'_F}\sqrt{2-m_F} < m'_F + \frac{1}{2}|m_F - \frac{1}{2} > \qquad (2.19)$$

The S_-B_{+DC} matrix element is

$$\Omega = \frac{\mu_B}{\hbar}g_s|\frac{B_{DC}}{2}|\frac{1}{2}\sqrt{2+m'_F}\sqrt{2+m_F} < m'_F - \frac{1}{2}|m_F + \frac{1}{2} > \qquad (2.20)$$

2.5 $\pi/2$ Pulses

The application of Rabi flopping to an atomic clock is illustrated by Figure 2.6 using the Bloch sphere formalism [7]. The green lines indicate the cardinal axes, while the red and blue lines represent the excited and ground states on the z-axis. The system begins in the ground state, so the orange state vector points along the -$\hat{z}$ direction. After an RF $\pi/2$ pulse, the system is put into a superposition of the ground and excited states. If the detuning is equal to 0, the vector stays still. If the detuning is off-resonance, then there will be precession at a frequency equal to the detuning. After a second RF $\pi/2$ pulse, if the detuning was on resonance, the system will be placed in the excited state, so the state vector will point along the $\hat{z}$ axis, but if there was precession between the $\pi/2$ pulses, there will be an uneven number of atoms in the two states, requiring a correction to the detuning.

The populations of the the two states can be seen using the Stern-Gerlach method. A magnetic field gradient acts as a spin selector to separate the atom populations based on their intrinsic quantum numbers, allowing us to separately image the ground state atoms and the excited state atoms.
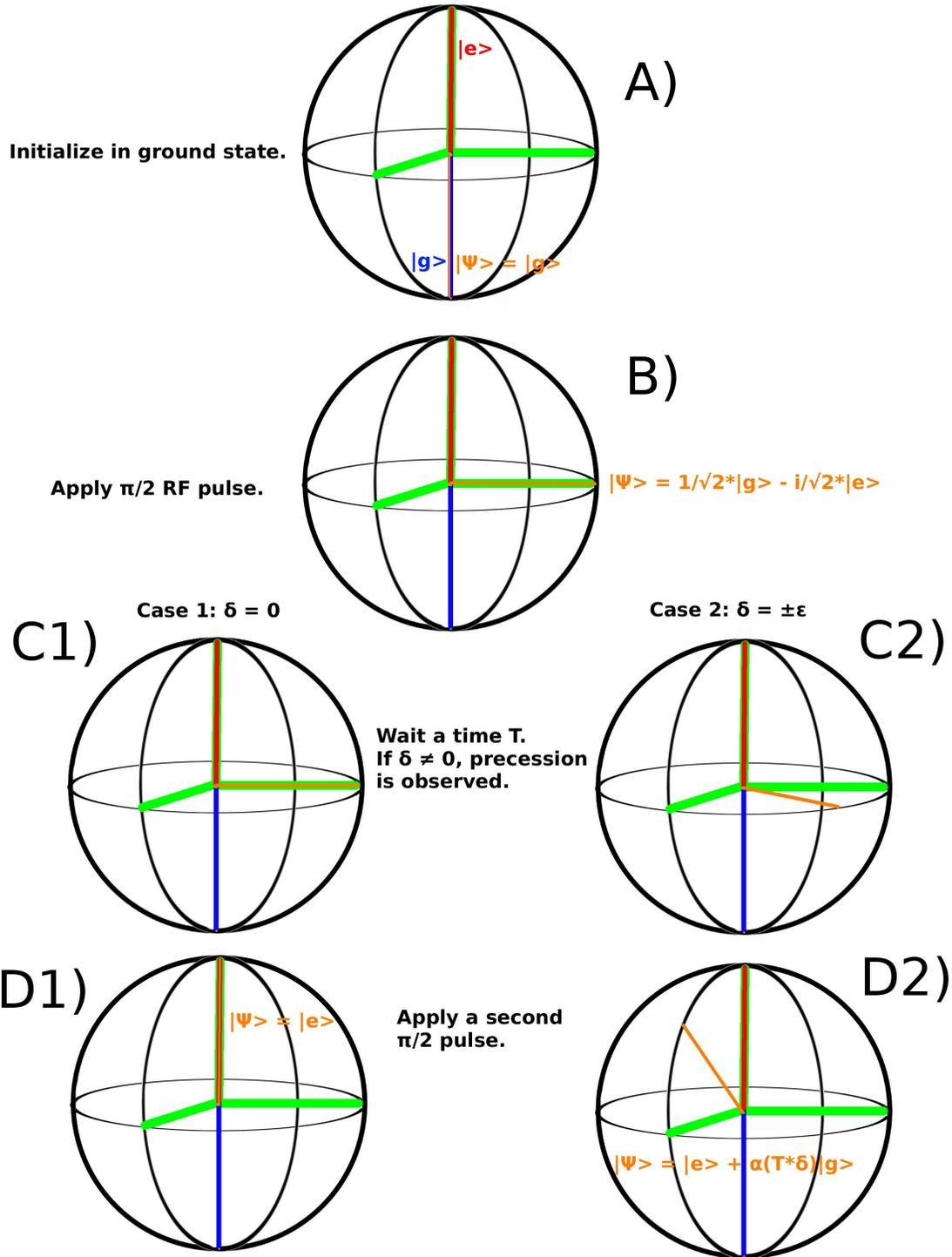
A)

|e>

Initialize in ground state.

|g> |Ψ> = |g>

B)

Apply π/2 RF pulse.

|Ψ> = 1/√2*|g> - i/√2*|e>

Case 1: δ = 0

C1)

Wait a time T.
If δ ≠ 0, precession
is observed.

Case 2: δ = ±ε

C2)

D1)

|Ψ> ≈ |e>

Apply a second
π/2 pulse.

D2)

|Ψ> = |e> + α(T*δ)|g>

Figure 2.6: Bloch sphere representation of Rabi flopping application to atomic clocks. The atoms begin in the ground state A), then a $\pi/2$ pulse places them in a superposition of states B). The system waits a time T. If the detuning $\delta \neq 0$, the state vector precesses at δ C2), else it will not change C1). After time T, a second $\pi/2$ pulse is applied. If $\delta = 0$, the atoms will be in the excited state D1), else there will be some inequality in the population D2).

2.6 Optical Pumping

Optical pumping can be used to place populations of atoms in a specific state. Consider a cloud of atoms, all in various energy states. When σ^+ polarized light (light polarized such that the AC magnetic field is circularly polarized) is applied to this atomic cloud, the atoms in the $|S, F = 2, m_F = -2>$ state get excited up to the $|P, F = 2, m_F = -1>$ state, per selection rules: $\Delta L = \pm 1$, $\Delta F = 0, \pm 1$, $\Delta m_F = +1$. Now, the atom can spontaneously emit a photon and decay back to the $|S, F = 2, m_F = -2>$ state, in which case optical pumping would make it return to the $|P, F = 2, m_F = -1>$ state, or the atom can decay to the $|S, F = 2, m_F = -1>$ state. In this way, the atoms eventually reach the $|S, F = 2, m_F = 2>$ state. At this point, there is no next state which would satisfy the selection rules, and so the atoms stay in the $|S, F = 2, m_F = 2>$ state. Figure 2.7 illustrates the process. With optical pumping, we can concentrate the population of the atoms to occupy a specific state, giving us more atoms to work with in our experiment.
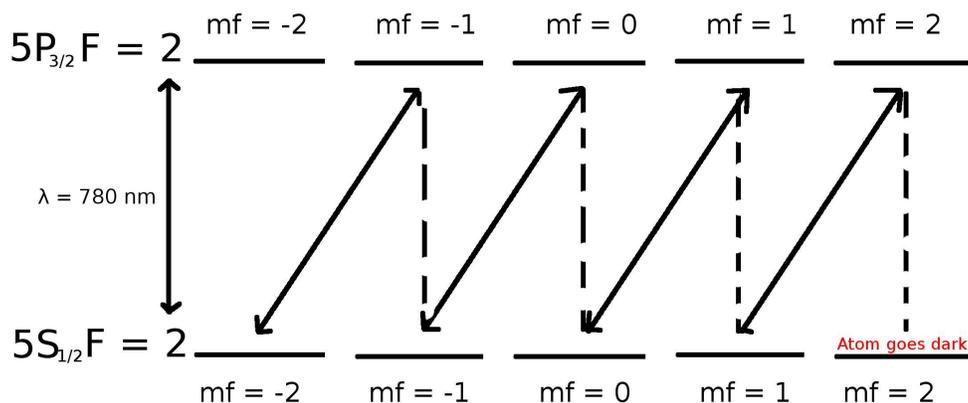

Figure 2.7: Diagram for optical pumping. The atoms get continuously excited until a transition can no longer be made, at which point the atoms go "dark" and can no longer absorb or emit photons.

3 Experiment

The experimental set-up required building a circuit to produce the $\pi/2$ RF pulses, as well as creating an RF antenna to emit the pulses. The circuit and antenna had to be optimized so that signal reflections from the antenna would not damage the circuit, requiring impedance matching. We also installed and fine-tuned an optical dipole trap to trap the ultra-cold atoms. With the trap in place, we attempted to observe Rabi-flopping using a signal generator to sweep through frequencies to find the resonant frequency. We also attempted to observe spin-selective imaging with atoms in the magnetic trap. We used adiabatic cooling to lower the temperature of the atoms.

3.1 RF Circuit

The $\pi/2$ RF pulses are needed to operate the atomic clock. They disturb the atoms that are initialized to a ground and state and place them in a superposition of states, and the pulses can then be used to probe the system to see if any precession has occurred. The circuit that will be used to produce the $\pi/2$ pulses is shown in Figure 3.1. The atomic clock will only use part of the circuit. A signal generator creates an RF signal, with a frequency near 460 MHz, the resonant frequency of ^{39}K. The signal is sent to the variable voltage attenuator, which allows control of signal's amplitude. The signal then goes to a TTL switch. The switch is used to temporarily turn off the signal leaving the switch without having to turn off the actual RF source. After the switch, the signal is amplified before entering the directional coupler, which has an RF antenna as the load.

3.2 RF Antenna

The RF signal is ultimately radiated by an RF antenna like the ones in Figure 3.2. The antenna consists of a stripped BNC cable with a resistor soldered on to adjust the impedance.
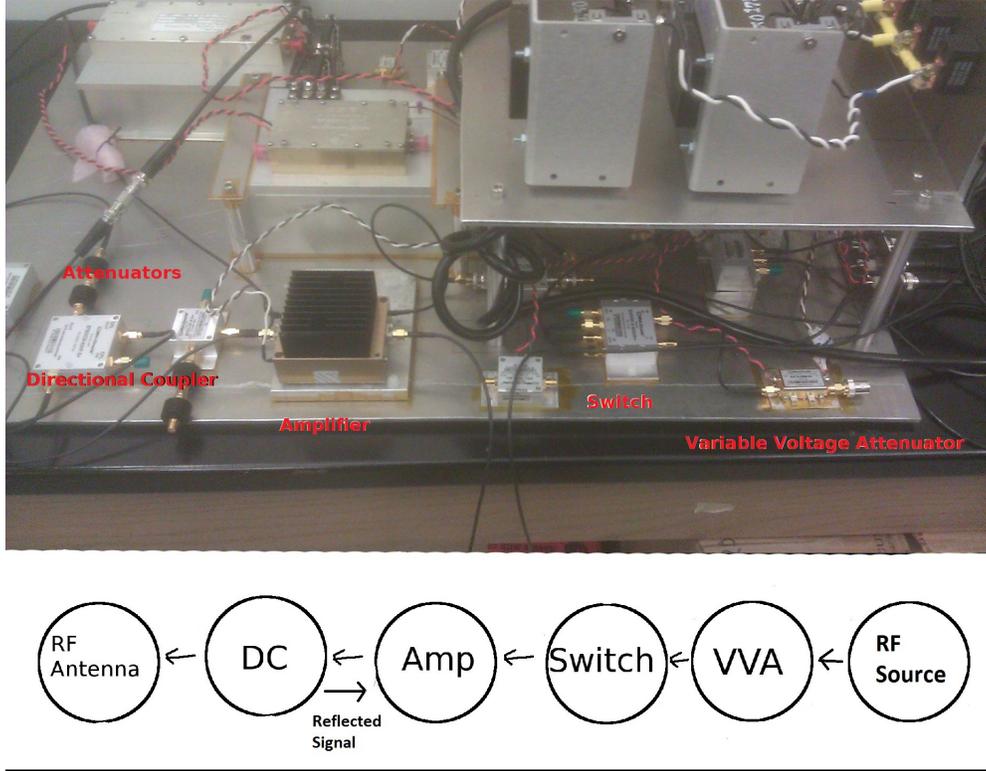
Figure 3.1: Image of the RF Circuit and its circuit diagram. The path of the RF pulse to the antenna is shown below the actual picture

The impedance matching is critical in reducing reflections from the output [8]. Reflections can cause harm to the circuit, particularly the amplifier, and so it is imperative to have the output impedance as close to 50Ω as possible. Approximating the antenna to a circular loop, and using Ampere's Law, the magnetic field from the loop is given by Equation 2.11. The flux through the loop is then

$$\Phi \propto \frac{\mu_0 I}{2R}\pi R^2 = \frac{\mu_0 \pi I R}{2} \tag{3.1}$$

With an antenna of approximate radius 5 cm and an antenna of approximate radius 1.5 cm, I measured the signal output using the pick-up coil. The ratio of V_{rms} from the larger coil compared to the small coil was about 1.86, which is proportional to the ratio of fluxes through the antenna. Then,

$$\frac{\Phi_l}{\Phi_s} = \frac{\frac{\mu_0 \pi I_l R_l}{2}}{\frac{\mu_0 \pi I_s R_s}{2}} = \frac{I_l}{I_s} \frac{R_l}{R_s} \simeq 1.86 \tag{3.2}$$

Solving for the currents, $I_l = 0.66 \ I_s$. So, the signal from the smaller antenna is stronger than the signal from the larger antenna, and thus better to work with. The antenna cannot be made too small, however, because that would limit the amount of atoms that could be successfully affected with the $\pi/2$ pulse.
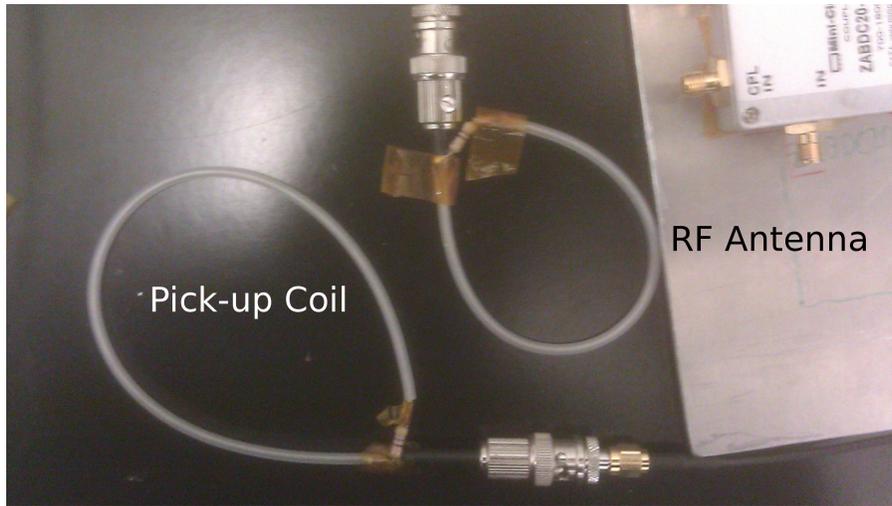

Figure 3.2: Two RF Antennae: one is used as a pick-up coil. The larger antenna was used to qualitatively measure the signal output from the smaller transmitting antenna.

3.3 Coupler Behavior

The RF antenna is attached to a directional coupler. The directional coupler sends part of the input signal to the output, and part to the coupled output. If the output impedance is not properly set to 50Ω, there will be a reflection from the output. The reflected signal needs to be minimized to prevent damage to the amplifier. To determine what the reflected signal is based on the output signal, I sent a varying signal to the directional coupler in the OUT port, and measured the CPL OUT and the IN signals. A plot of CPL OUT vs. input signal (in this case, the OUT port) is shown in Figure 3.3. From the linear fit, I conclude that the
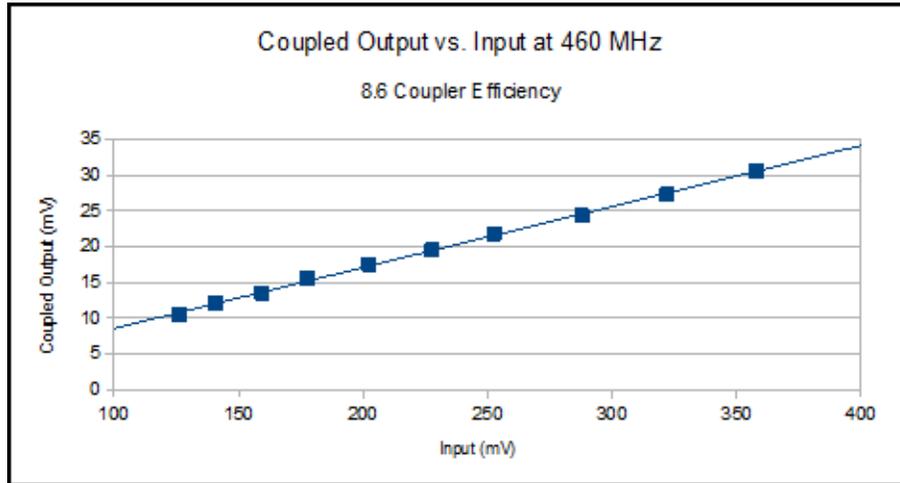
Figure 3.3: Plot of Coupled Output vs. Input. The signal coming out of the coupler linearly increases with the signal from the OUT port, i.e. reflections.

CPL OUT is 8.5% of the signal going into the OUT port. Thus, in normal operation, when an input signal goes into the IN port, whatever comes out of the CPL OUT port is 8.5% of the signal reflected from the antenna attached to the OUT port. What matters is the power reflection, however. We desired a power reflection under 25% maximum. Initially, we had 45% reflection. With a 3dB attenuator, however, we were able to drop the power reflected to 5.4%, well within a safe range of operation. With a 50Ω load on the directional coupler, the theoretical 'zero reflection,' we still had 4% reflection, so that is the best we can hope to achieve.

The frequency of the RF signal affects the reflection of the output signal as well. Figure 3.4 gives the plot of the reflected signal's root-mean-square value as a function of input frequency. The antenna is more optimized for 440 MHz rather than 460 MHz, but it is still functional for our purposes at 460 MHz.

With the full set-up of the RF circuit at 460 MHz, the amplified signal coming out of the amp is 245 mW in power, and the reflected signal from the antenna is 21.9 mW, a safe 8.9% reflection.
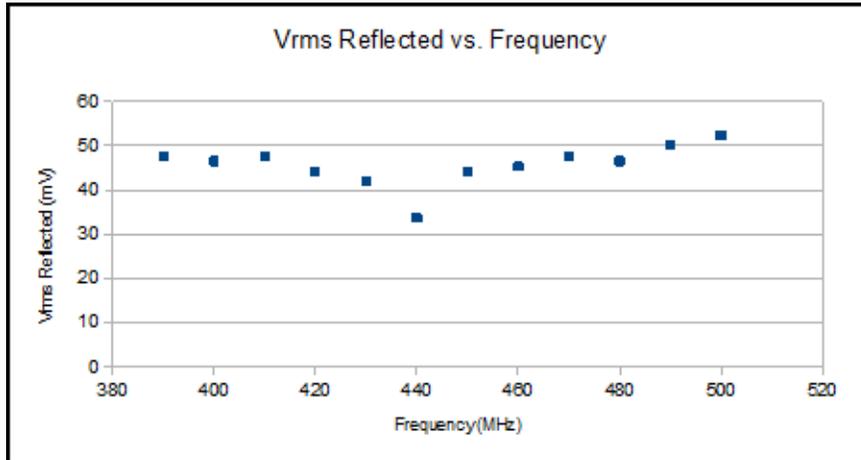
Figure 3.4: Plot of V_{rms} reflected vs. Frequency. The smallest reflections occur at 440 MHz.

3.4 Optical Dipole Trap

The atoms are first trapped in a magneto-optical trap, and then moved from the MOT to a dipole trap. The process is handled by a program called AdWin, which allows us to control digital and analog signals being sent to the various experimental modules.

Figure 3.5 shows the top section and Figure 3.6 shows the initial set-up of the optical table. The beam path is drawn on the figures. To give more control over the beam, an acousto-optic modulator was installed, shown in Figure 3.7. The AOM uses an incident RF signal to change the index of refraction of material inside it, allowing modulation of the signal transmitted through the AOM. In this way, we can adjust the phase and intensity of the laser. A telescope made with cylindrical lenses was also aligned in order to increase the beam power. Figure 3.8 shows where the beam exits the vacuum cell. A mirror retroreflects the beam onto itself, which doubles the field of the trap and consequently quadruples the power, giving us a stronger trap.
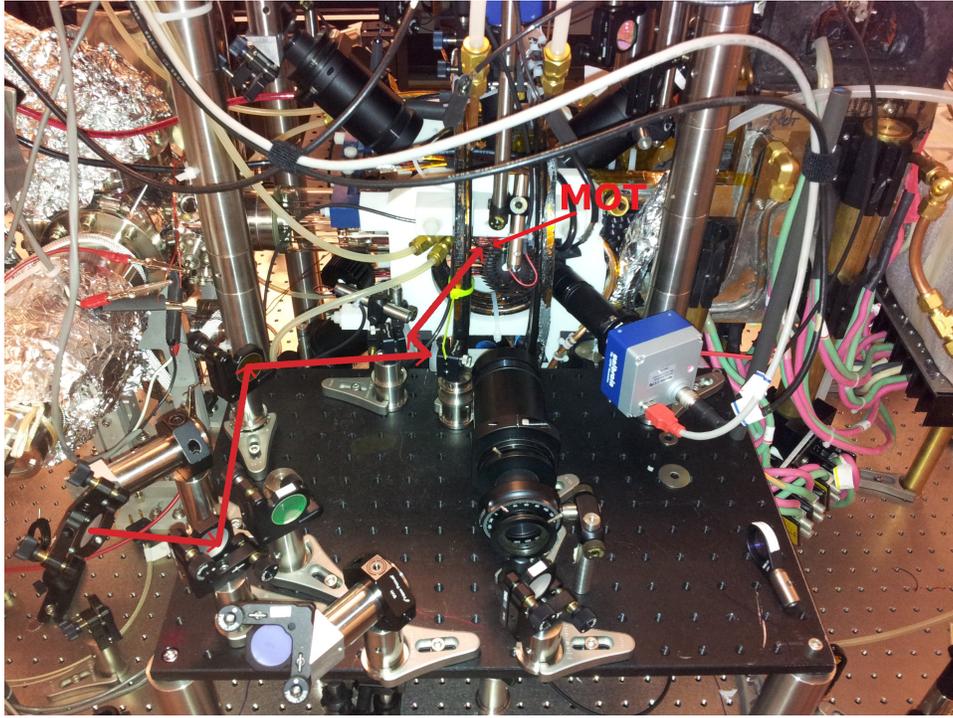
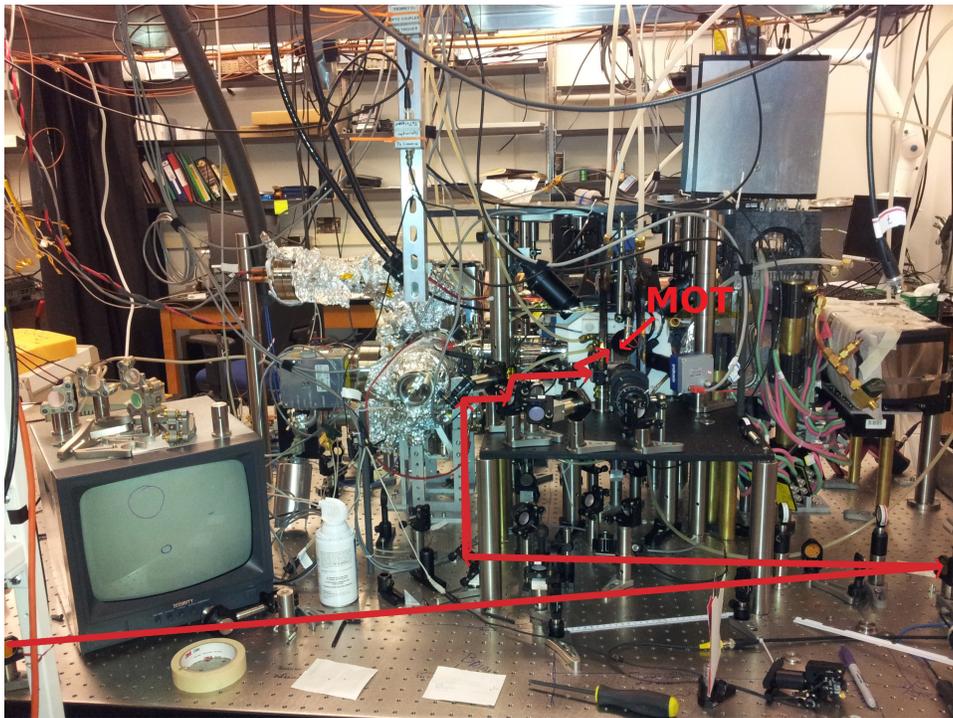Figure 3.5: Image of the top part of the optics table. The beam path is traced.

Figure 3.6: Image of the entire optics table. The telescope on the lower section collimates the beam. The beam path is traced.
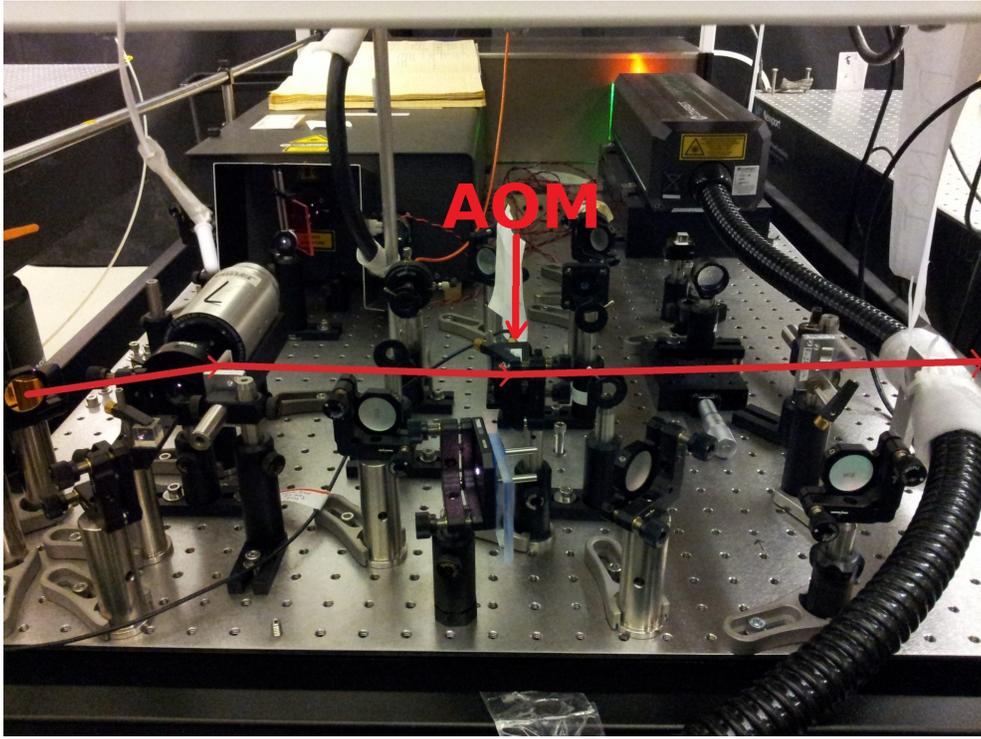
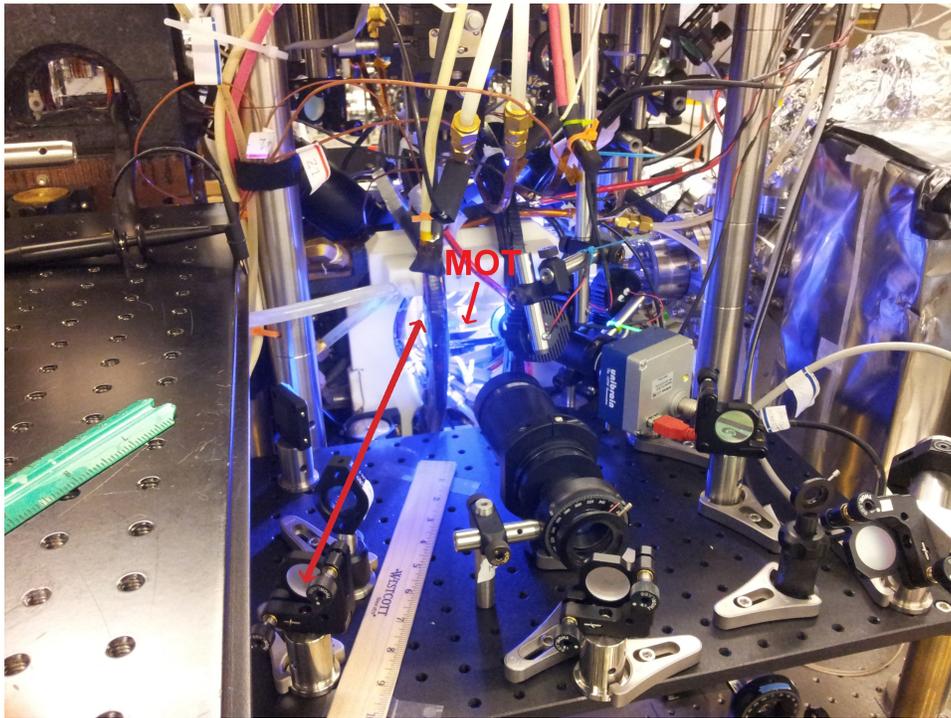Figure 3.7: Placement of the AOM and cylindrical telescope. The beam path is traced.

Figure 3.8: The other side of the vacuum cell. The beam is retroreflected to gain more power. The beam path is traced.

Trapped Rubidium atoms can be seen in Figure 3.9. The colors indicate density, where red corresponds to many atoms per volume and blue corresponds to few. The left half of the image shows atoms in a regular dipole trap, trapped along the length of the laser. The right part of the image shows atoms in a latticed dipole trap. The lattice is formed by crossing the laser beam to create interference. The atoms are trapped in areas of high-intensity in the interference pattern, creating a more compact trap.
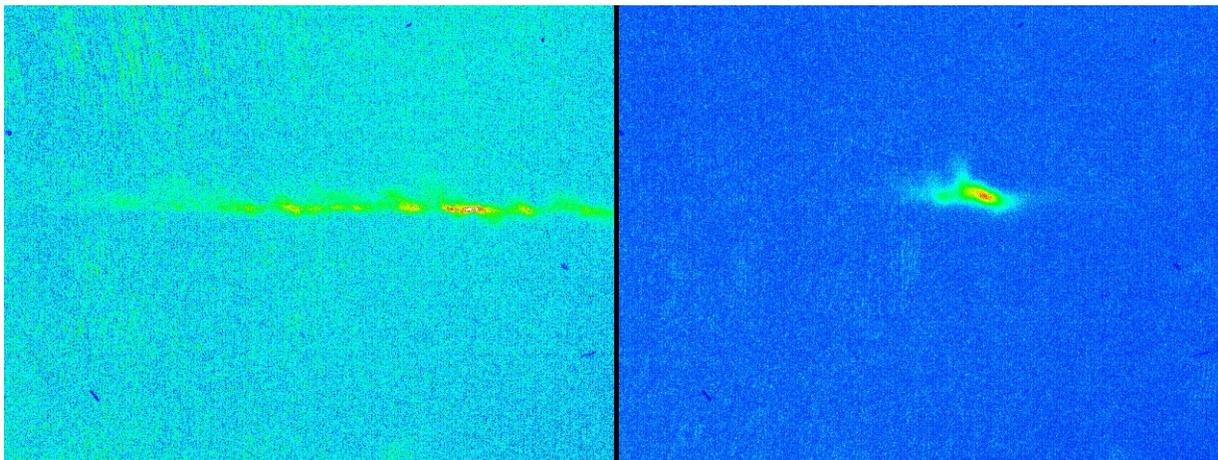

Figure 3.9: Imaged atoms suspended in the dipole trap on the left, and in the latticed dipole trap on the right. The lattice prevents the atoms from axially spreading, keeping them confined to a smaller area.

Eventually, the small AOM will be replaced with a larger, more powerful one. In order to power the AOM, we need an appropriate circuit. Figure 3.10 shows the current status of the circuit. The amplifier is powered by the power supply, and soldering work needs to be done to power the switch.

3.5   Rabi Flopping

To operate the atomic clock, we'd like to see the atoms Rabi flop from one energy state to another. In order to observe Rabi flopping, we need to emit RF pulses, with controllable pulse duration and signal frequency. The first approach was to use the "Burst" function on the signal generator. This allowed us to create pulses with a set number of cycles, as
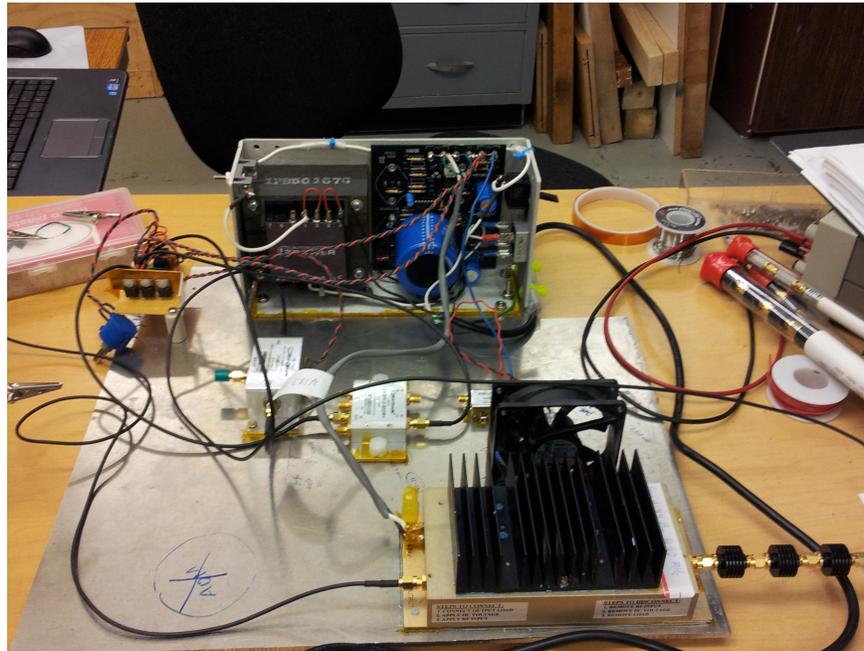
Figure 3.10: The AOM amplifier circuit.

well as a set frequency of the bursts. Figure 3.11 shows the signal coming out of the signal generator.
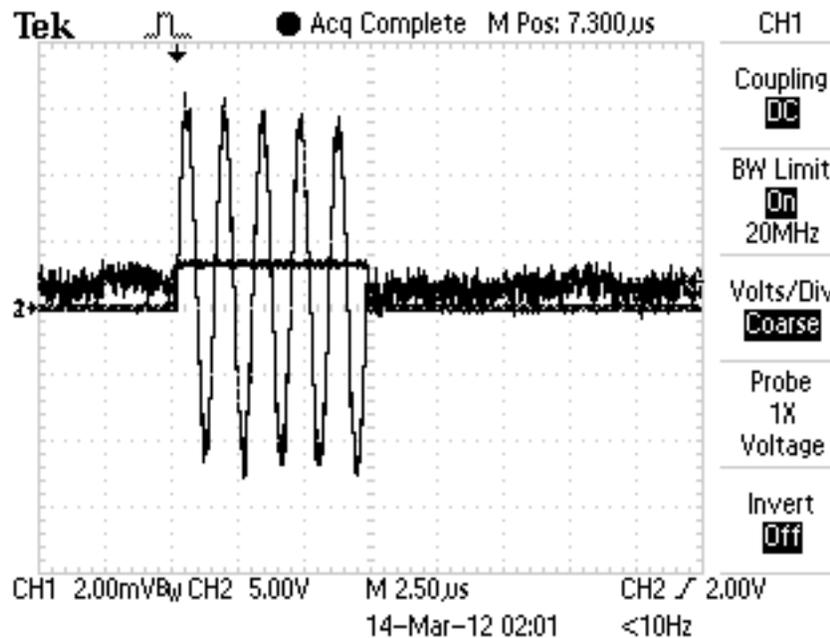

Figure 3.11: RF burst output from signal generator.

Figure 3.12 shows the signal received by the pickup coil. There is a strange decay residue

after the burst, possibly caused by reflections of the signal from the vacuum cell.
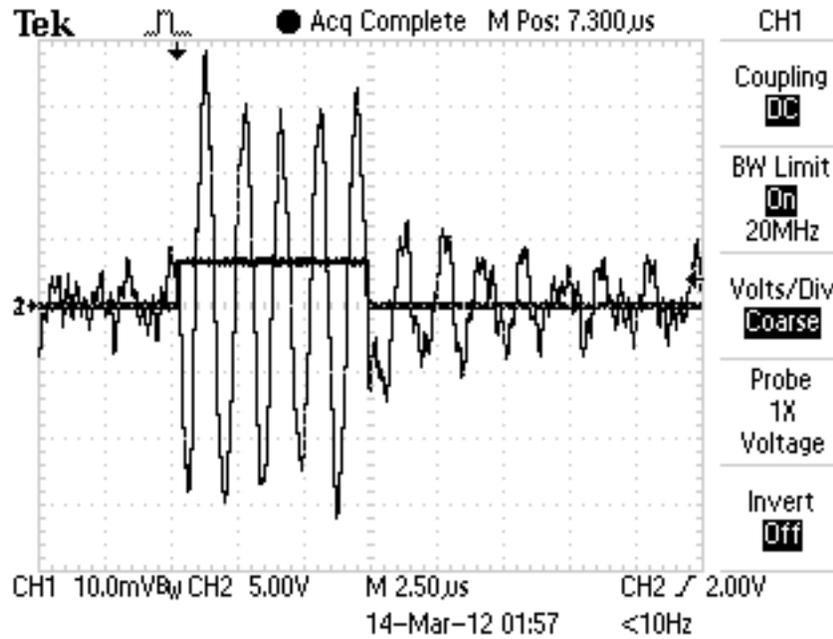

Figure 3.12: RF burst signal picked up by coil. The residue signal after the end of the burst is possibly due to the signal reflecting inside the cell.

Unfortunately, the "Burst" function is not ideal, as the burst time cannot be adjusted, only cycle number, We decided to switch to amplitude-modulation pulses. By sending a signal from the AdWin as a carrier wave, we can modulate the RF signal so that it is only on for as long as the carrier period. Figure 3.13 shows the AM signal from the pick-up coil. It is on for 3ms and then the AdWin turns one of the TTL voltage switches off so the atoms stop receiving RF signals. The signal generator also has a "Sweep" function that allows us to comb through frequencies to find the exact resonant frequency.

We attempted to use the Stern-Gerlach method to separate the atoms by state and image them, but results were inconclusive. Either the magnetic field from the antenna was not strong enough or the atoms were too hot.
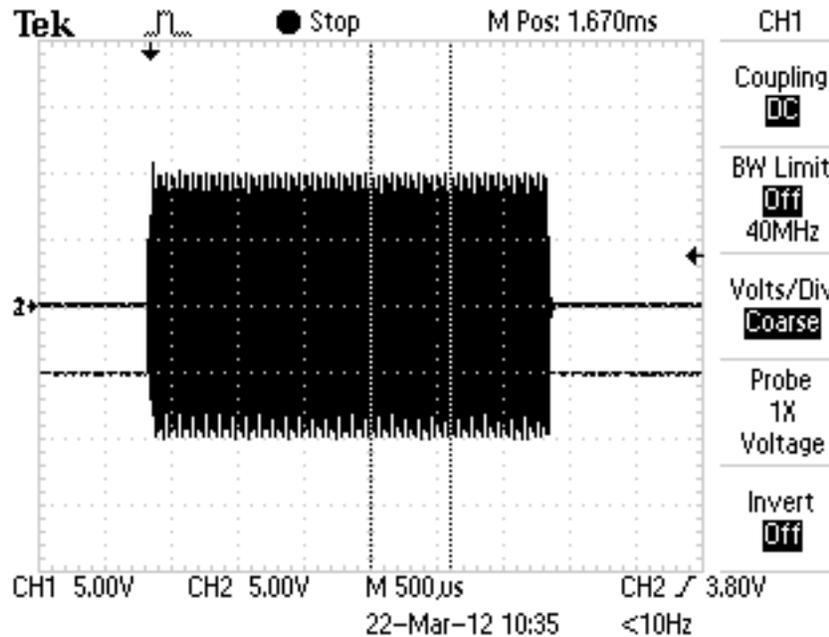
Figure 3.13: Amplitude-modulated RF pulse. The pulse is 3ms long, with a frequency of 700 kHz.

3.6   Spin-Selective Imaging

The Rabi flopping was not working with the Stern-Gerlach method, so we decided to try observing spin-selective imaging using optical pumping. We can observe periodic behavior of the atoms flopping back and forth between the pumped state and the initial state, since the magnetic trap acts as a spin selector. The magnetic trap only traps $|F = 2, m_F = +2>$ atoms. $|2, -2>$ and $|2, -1>$ atoms are repelled by the trap, while $|2, 0>$ atoms are unaffected. $|2, 1>$ atoms are trapped, but not strongly, and they fall out of the trap due to gravity. So, only $|2, 2>$ atoms remain. Figure 3.14 shows magnetically trapped atoms without any optical pumping on the left, and magnetically trapped atoms with optical pumping on the right.
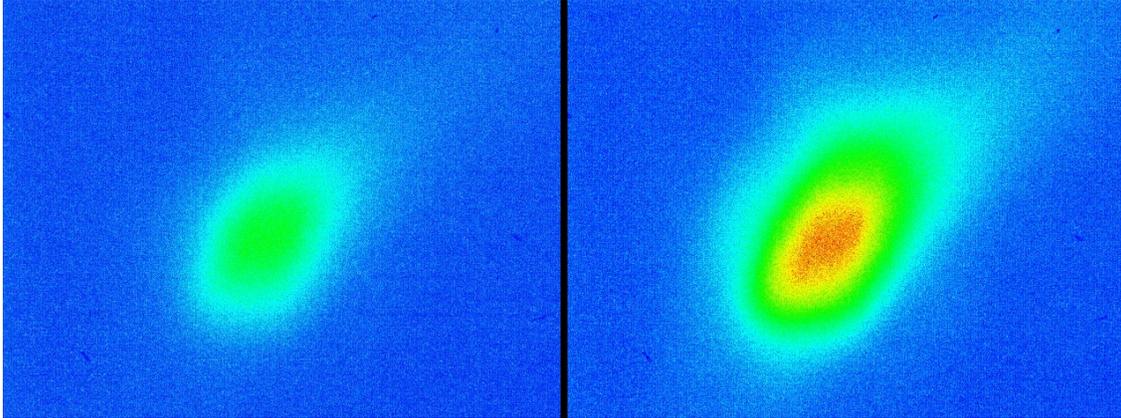
Figure 3.14: $|F = 2, m_F = +2>$ atoms without optical pumping on the left, with optical pumping on the right. There are significantly more atoms trapped with optical trapping than without.

There is a very noticeable increase in atom population due to optical pumping. By optically pumping, we put a higher percentage of the Rubidium atoms into the $|2,2>$ state, increasing our population of trapped atoms. In arbitrary units, the "amount" of atoms trapped without optical pumping was 1.5×10^9, while with optical pumping, we had 3.5×10^9, a factor of 2.3.

The procedure is to put the atoms in the $|2,2>$ state with optical pumping, and then image the atoms. We then apply a Rabi frequency RF pulse of 350 kHz to the atoms, between the optical pumping and imaging stages. We should see a change in signal as the atoms change their m_F value. The magnetic field has a gradient of 20 G/cm, with the zero-point of the magnetic field being the center of the trap, and increasing away from the center. Figure 3.15 gives a sketch of how the signals will turn off and on during the spin-selective imaging procedure.

We observed little to no effect from the RF pulses. We first checked to make sure the atoms were receiving the RF pulses. Without the RF signals, when we turned the trap back on, the atoms were still trapped. With the antenna radiating RF signals, however, we saw that the atoms had evaporated when the trap was turned back on.

So the atoms were indeed receiving RF signals, just not strong enough to induce flopping.
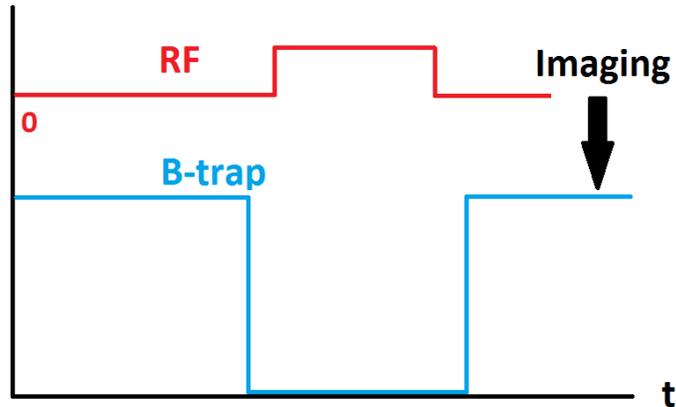
Figure 3.15: Signal representation of when the RF and B-trap are on during procedure. Imaging occurs after the RF is turned off.

We switched to a new antenna, which had 10 coils, in order to increase the strength of the magnetic field from the antenna. With a 10V peak-to-peak input signal, the antenna was outputting 904 mV peak-to-peak at 700 kHz. A 10.3 Ω resistor connected to the antenna gives a current of 43.9 mA, and the antenna has a radius of 3.875 cm. At roughly 3cm away from the antenna, and multiplying by 10 due to the coil number, this corresponds to a magnetic field strength of 35 mG, where previously with the single coil RF antenna we had 8.47 mG. This antenna has not been tested yet with the optical pumping procedure.

We also made temperature measurements to make sure the atoms were cold enough. We turned the trap off for a certain time of flight, and imaged the atoms. By making a Gaussian plot of the intensity and measuring its width, we can plot the width in centimeters versus time of flight in seconds. From this velocity we can calculate the temperature. Initially, our atoms were at 33 μK. We used adiabatic cooling to cool the atoms, and remeasured the temperature. Figure 3.16 compares the cloud width against time of flight for atoms without and with adiabatic cooling.
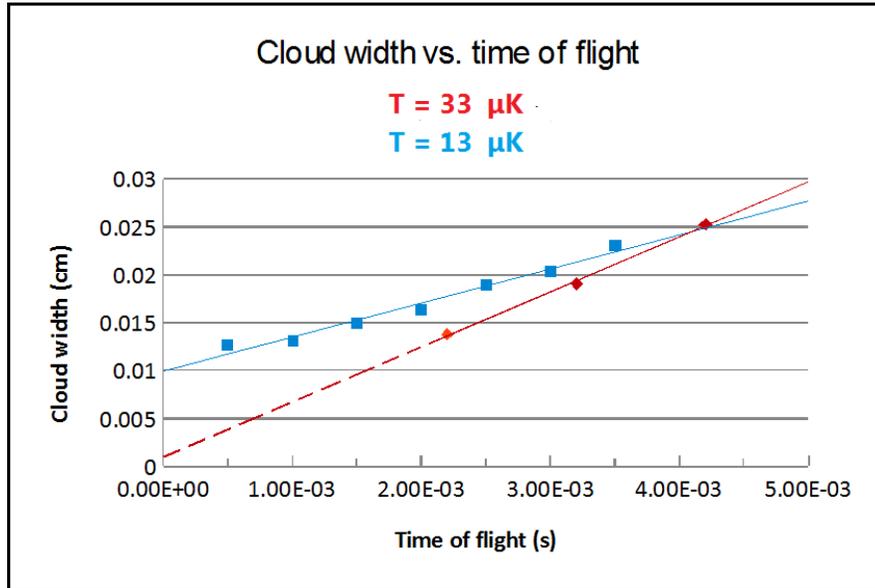
Figure 3.16: Gaussian width vs. time of flight for trapped atoms without adiabatic cooling (red) and with adiabatic cooling (blue). The temperature drops from 33μK to 13μK.

Adiabatic cooling is achieved by slowly ramping down the power of the trap, allowing the more energetic, and hotter, atoms to escape the trap, leaving us with colder atoms. The colder atoms get cooled even further since there are fewer energetic atoms to heat them up. The caveat is that there are less atoms to work with. With cooling, our atoms were at 13 μK.

4 Conclusion and Outlook

We have set up the optics for the dipole trap, and have observed trapped atoms. We can cool the atoms down to 13 μK, which is within working range for the atomic clock. We have attempted to observe Rabi flopping in the atoms, but spin-selective imaging methods have not yet worked successfully. The next step is to use an antenna with more coils, which can produce a stronger radio frequency signal.

We need to observe Rabi flopping in the atoms, which is an integral part of the atomic clock operation. Once we have figured out the best way to send RF signals to the atoms, we

can set up the atomic clock system for Potassium atoms. A field-programmable gate array will be used to control the signal generator producing the RF pulses, and a MATLAB script will be used to analyze the imaged atoms to figure out how far off-resonance the detuning is. In addition, once the acousto-optic modulator circuit is complete, the larger AOM can be installed in the optical circuit to provide more power to the trap.

Once the atomic clock is working, we can observe inter-atom interactions. By adjusting the magnetic Feshbach resonance, we can control the hyperfine structure of the atom and calculate the effect it has on the clock's timing. Another possible application of the atomic clock is as a magnetic gradiometer, to measure magnetic gradients based on their effect on the clock.

Acknowledgments

References

[1] F. G. Major, *The Quantum Beat: The Physical Principles of Atomic Clocks*, Springer, 1998.

[2] "NIST-F1 Cesium Fountain Atomic Clock." NIST.
http://www.nist.gov/pml/div688/grp50/primary-frequency-standards.cfm

[3] G. K. Campbell et. al, "Probing Interactions Between Ultracold Fermions," *Science.* **324**, 5925. (2009)

[4] C. Chin et. al, "Feshbach resonances in ultracold gases," *Reviews of Modern Physics.* **82**. (2010).

[5] C. J. Foot, *Atomic Physics*, Oxford Master Series In Atomic, Optical, and Laser Physics, 2005.

[6] E. Hecht, *Optics*, 4th edition, Addison Wesley, 2001.

[7] R. Feynman, F. Vernon, and R. Hellwarth, "Geometrical Representation of the Schrodinger Equation for Solving Maser Problems," *Journal of Applied Physics.* **28**, 1. (1957).

[8] S. Y. Mak and K. Young. "Determination of the self-inductance of a metal ring." *Phys. Educ.* **21**. (1986).